Interlayer co-chemistry of homologous ion stabilizer and microenvironmental molecular regulator for high-performance zinc-ion storage

Keyi Chen,[a] Quan Zong,[a]* Yuqing Ji,[a] Helixin Jiao,[a] Qiaoling Kang,[a] Qilong Zhang,[b] Shuang Zhou,[d] Qianqian Wang,[e] Guoying Wei,[a] Zhihao Lou,[a] Anqiang Pan[c, d]*

a College of Materials and Chemistry, China Jiliang University, Hangzhou 310018, Zhejiang, People's Republic of China

b State Key Lab of Silicon and Advanced Semiconductor Materials, Zhejiang University, Hangzhou 310027, Zhejiang, People's Republic of China

c School of Materials Science and Engineering, Xinjiang University, Urumqi 830017, Xinjiang, People's Republic of China

d School of Materials Science & Engineering, Central South University, Changsha 410083, Hunan, People's Republic of China

e School of Science, Huzhou University, Huzhou 313001, Zhejiang, People's Republic of China

Corresponding authors: E-mail: quanzong@cjlu.edu.cn (Q. Zong), pananqiang@csu.edu.cn (A. Pan)

Experimental section

Synthesis of (TEG, Zn)-VOH Hybrid Materials

All chemical reagents were used as received without further purification. Prior to synthesis, carbon cloth substrates were chemically activated by immersion in a mixed concentrated H_2SO_4/HNO_3 solution (v/v = 1:1) at 80 °C for 30 min, followed by thorough rinsing with deionized water until a neutral pH was attained. Subsequently, the cloth was ultrasonically cleaned in deionized water and ethanol sequentially, each for 30 minutes, to remove surface impurities and organic residues thoroughly, and then dried at 60 °C for later use. In a typical hydrothermal synthesis, 2 mmol of V_2O_5 (Aladdin, 99.5%) was dispersed in 80 mL of deionized water under vigorous magnetic stirring. Subsequently, 2 mL of 30 wt% H_2O_2 (Aladdin, AR) was added dropwise, and the mixture was stirred at room temperature for 30 minutes. Then, 10 mL of triethylene glycol (TEG) (Aladdin, 99.0%) aqueous solution was introduced into the above mixture, followed by stirring for another 15 minutes. Afterward, 1 mmol of $ZnSO_4 \cdot 7H_2O$ (Aladdin, 99%) was added and stirred for 30 minutes to obtain a homogeneous precursor solution. The resulting mixture along with a piece of pretreated carbon cloth was sealed in a 100 mL Teflon-lined stainless-steel autoclave and maintained at 120 °C for 6 hours. After the reaction, the carbon cloth was taken out, thoroughly washed with deionized water and ethanol, and finally dried under vacuum at 60 °C for 12 hours. The obtained (TEG, Zn)-VOH material grown on carbon cloth had an active mass loading of approximately 2 mg cm^{-2}.

Materials Characterization

The crystal structures of the samples were examined by X-ray diffraction (XRD, Rigaku D/Ultima

IV) using Cu Kα radiation (λ = 1.5418 Å). Thermogravimetric analysis (TGA) was carried out on a Netzsch STA 449 F3 thermal analyzer under an air atmosphere, with a heating rate of 10 °C min^{-1} from 30 to 600 °C, to assess mass evolution and thermal stability. Surface elemental compositions and chemical states were investigated by X-ray photoelectron spectroscopy (XPS, Thermo Scientific K-Alpha). The morphology and microstructural features were characterized using scanning electron microscopy (SEM, JSM-IT800) and transmission electron microscopy (TEM, JEM-2100F), both equipped with energy-dispersive X-ray spectroscopy (EDS) for elemental mapping analysis. Fourier transform infrared spectroscopy (FTIR, Thermo Fisher Scientific Nicolet iS5) was conducted in the wavenumber range of 600 to 4000 cm^{-1} to identify the functional groups. Electron paramagnetic resonance (EPR) spectroscopy was employed to probe the defect characteristics of the samples on Bruker A300.

Electrochemical Measurements

All electrochemical measurements were carried out using CR2032 coin-type cells assembled in ambient atmosphere. The freestanding carbon cloth loaded with active material was directly used as the cathode. A zinc foil (100 μm) served as the anode, a glass fiber membrane as the separator, and 80 μL of 3 M $Zn(CF_3SO_3)_2$ aqueous solution as the electrolyte. Cyclic voltammetry (CV) tests were conducted on an electrochemical workstation (CHI 760E, Chenhua) within a voltage window of 0.2 to 1.6 V (vs. Zn^{2+}/Zn). Electrochemical impedance spectroscopy (EIS) measurements were performed in the frequency range from 0.01 Hz to 100 kHz with an AC perturbation amplitude of 5 mV. Galvanostatic charge/discharge tests and galvanostatic intermittent titration technique (GITT) were performed on a Neware battery testing system (CT-4008, Shenzhen).

Theoretical calculations

All density functional theory (DFT) calculations were performed using the Vienna Ab initio Simulation Package (VASP).[1-2] The exchange-correlation interactions were treated with the Perdew-Burke-Ernzerhof (PBE) functional under the generalized gradient approximation (GGA) framework.[3-4] Core–valence electron interactions were modeled using the projected augmented wave (PAW) approach.[5] A plane-wave energy cutoff of 450 eV was employed, and Brillouin zone sampling was carried out using a 1×1×1 Gamma centered k-points. Structural relaxations were considered converged when the total energy and atomic forces were below 1.0×10^{-5} eV and 0.02 eV $Å^{-1}$, respectively. Long-range van der Waals interactions were incorporated via the DFT-D3 correction scheme.[6]

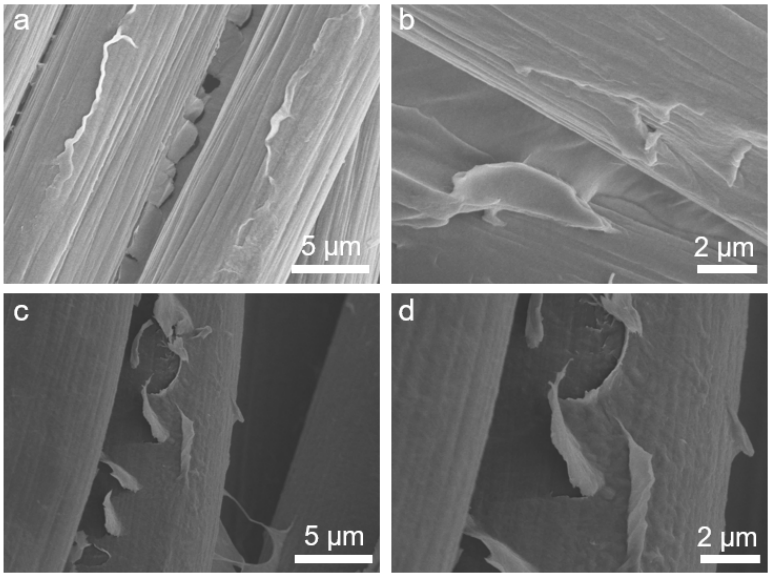

Fig. S1. SEM images of (a, b) VOH, (c, d) TEG-VOH.

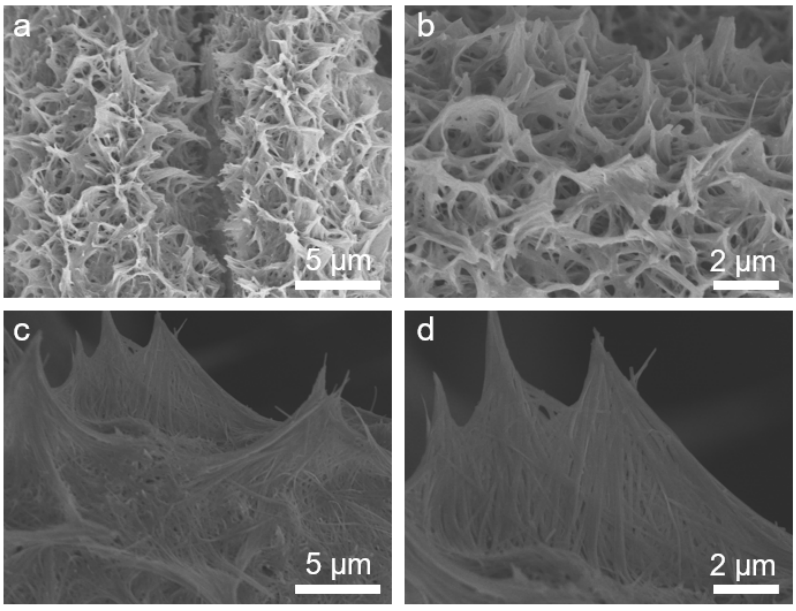

Fig. S2. SEM images of (a, b) Zn-VOH, (c, d) (TEG, Zn)-VOH.

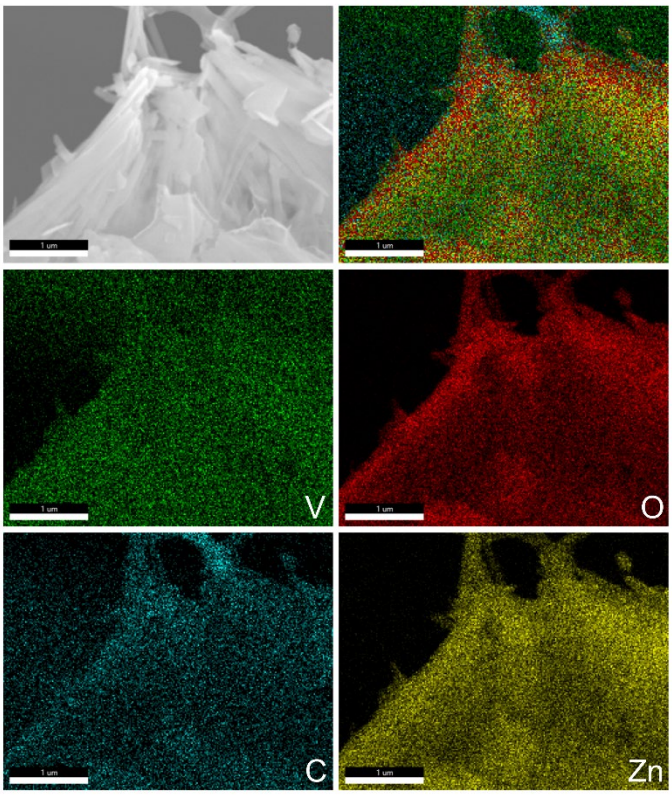

Fig. S3. EDS mappings of (TEG, Zn)-VOH.

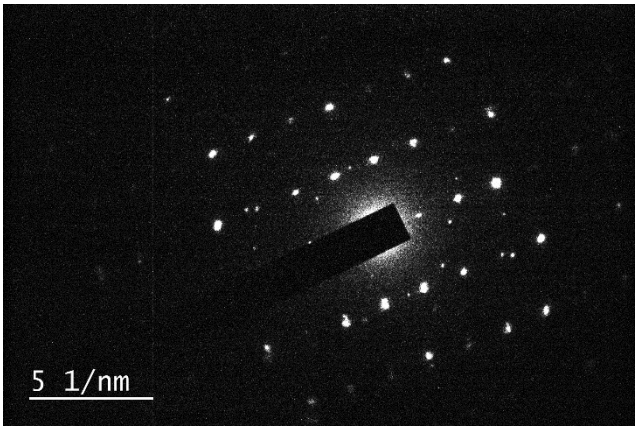

Fig. S4. SAED pattern of (TEG, Zn)-VOH.

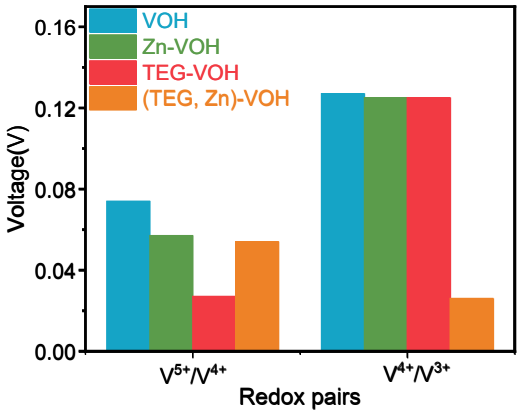

Fig. S5. Voltage gaps of all electrodes.

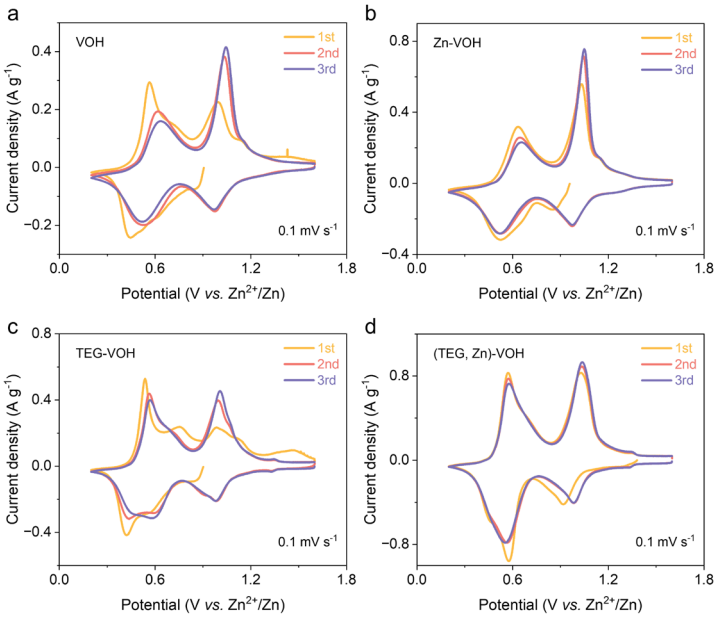

Fig. S6. The first three CV cycles.

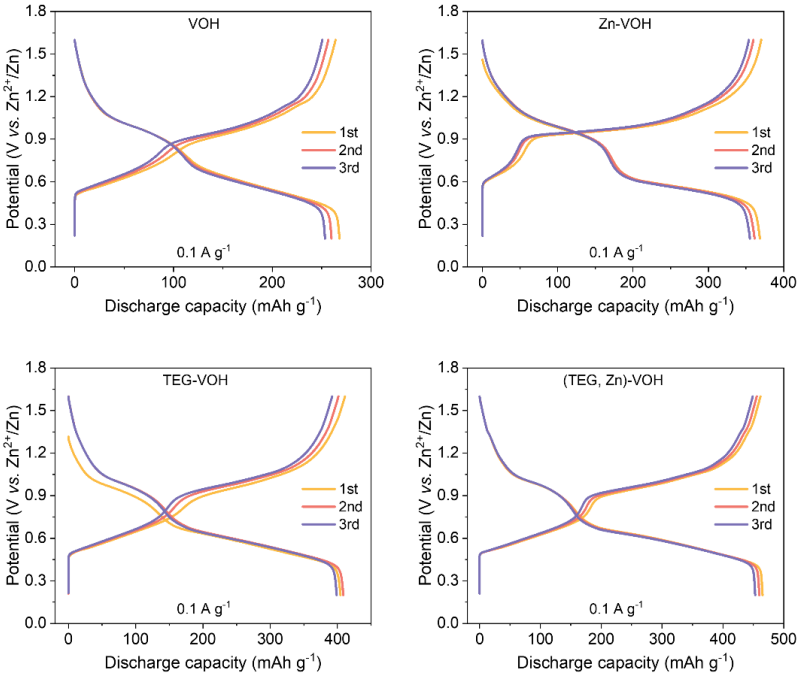

Fig. S7. The first three GCD cycles.

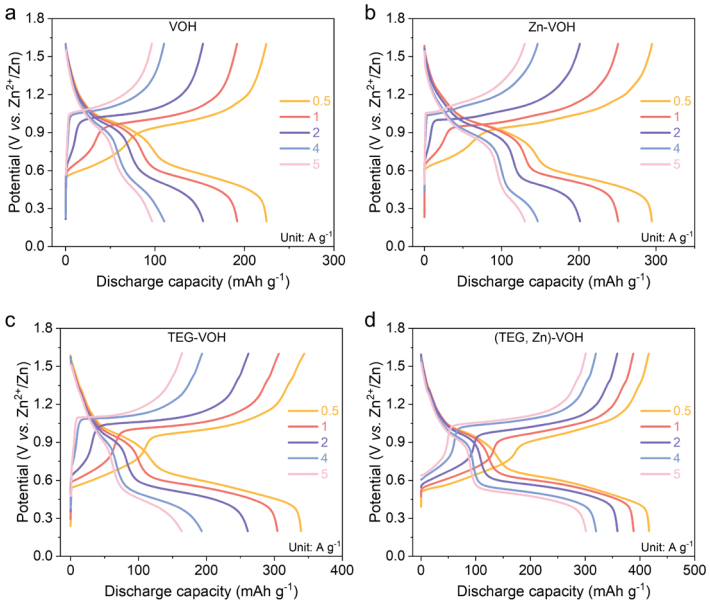

Fig. S8. Voltage profiles at various current densities.

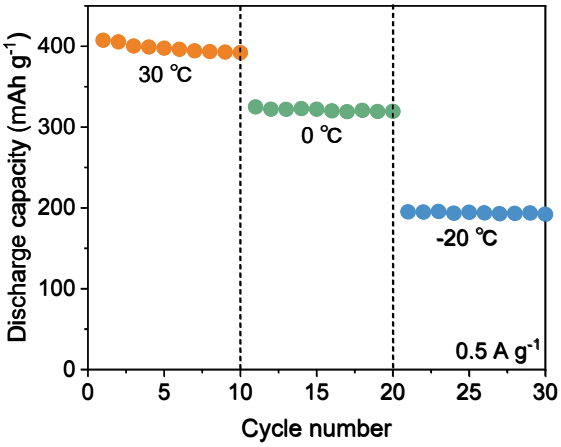

Fig. S9 Discharge capacity across a temperature range from 30 ℃ to -20 ℃.

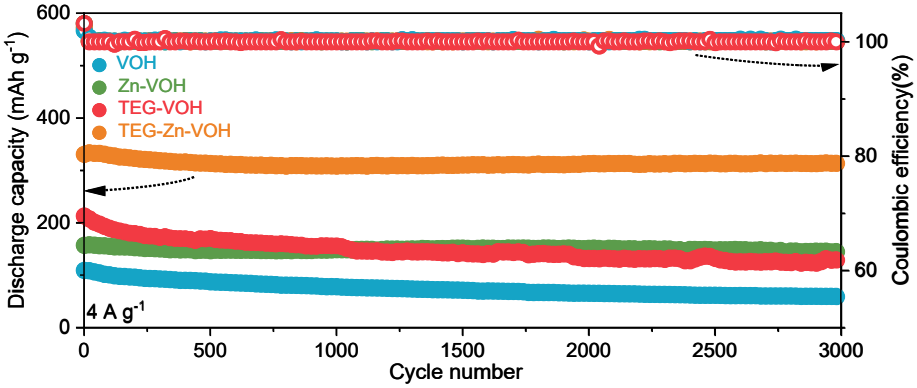

Fig. S10 Cycling performance at 4 A g^{-1}.

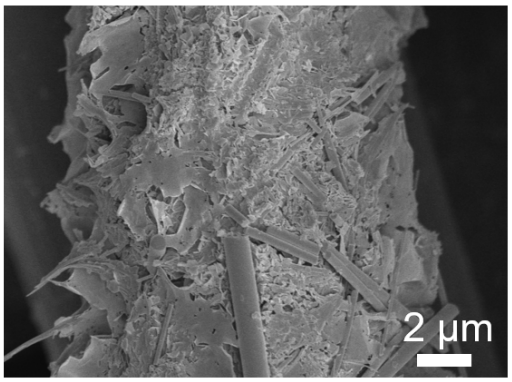

Fig. S11 SEM image of (TEG, Zn)-VOH after cycling.

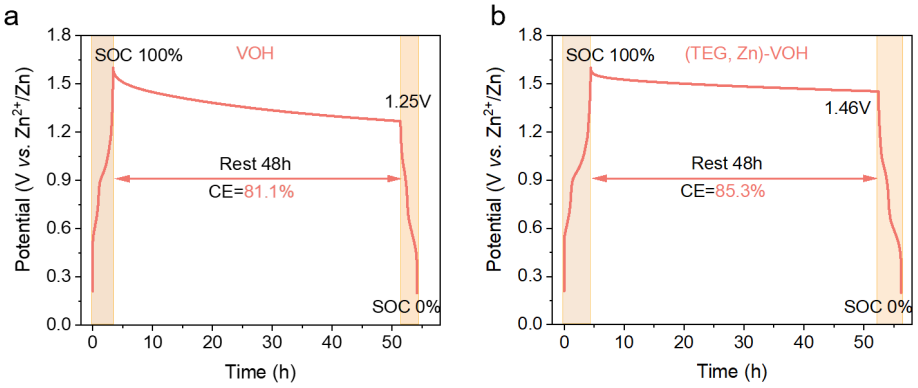

Fig. S12 Self-discharge behavior of a) VOH and b) (TEG, Zn)-VOH.

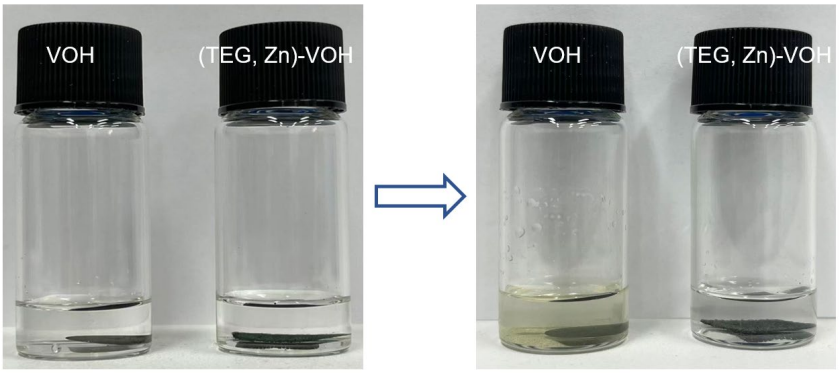

Fig. S13 Optical photographs of the electrolytes' color after soaking with the electrodes.

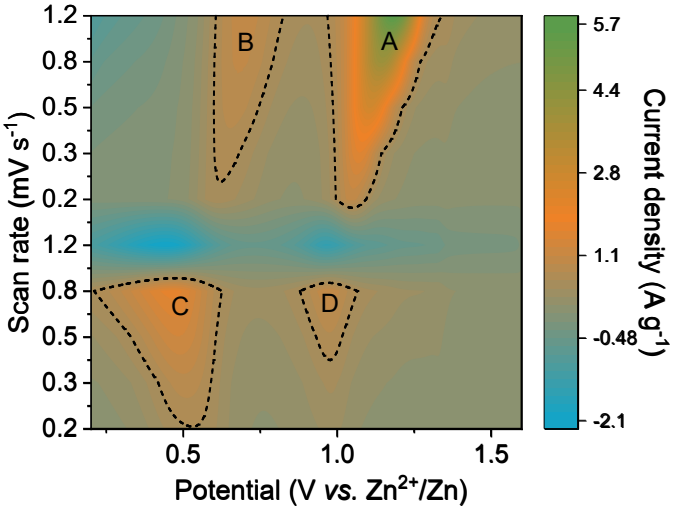

Fig. S14 CV contour of VOH.

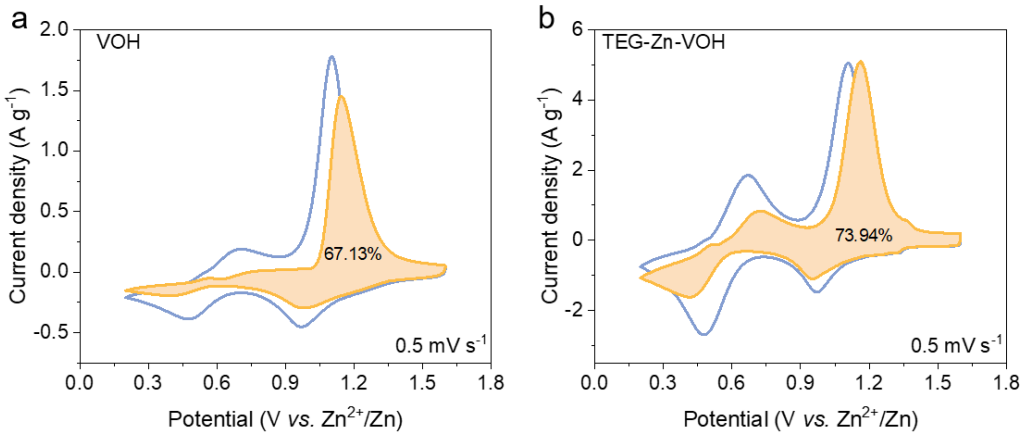

Fig. S15 Capacitive contributions of a) VOH and b) (TEG, Zn)-VOH at 0.5 mV s^{-1}.

The relationship between the sweep rate (v) and the peak current (i) can be described by the following equation:[7]

$$i=av^b$$

where a and b are adjustable fitting parameters. The value of b provides insight into the charge-storage mechanism, with b = 0.5 indicating a diffusion-controlled process and b = 1.0 corresponding to a surface-controlled behavior.

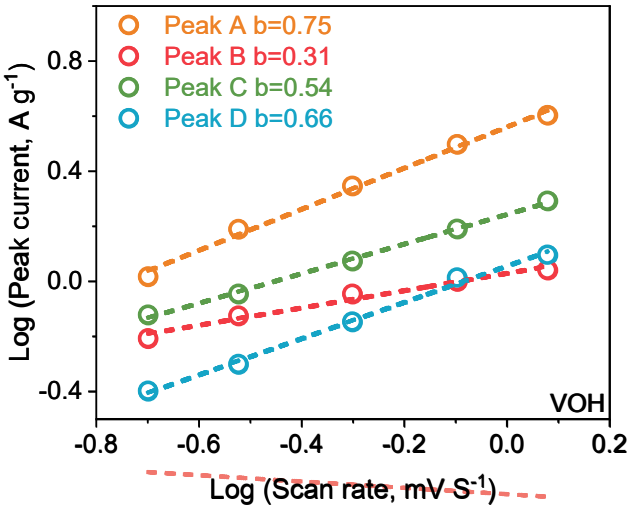

Fig. S16 b-values of VOH.

The capacitive contribution to the total current response can be quantitatively evaluated according to the following equation:[8]

$$i=k_1v+k_2v^{1/2}$$

where k_1v represents the current contribution arising from surface-controlled capacitive processes, while $k_2v^{1/2}$ corresponds to the diffusion-limited intercalation contribution.

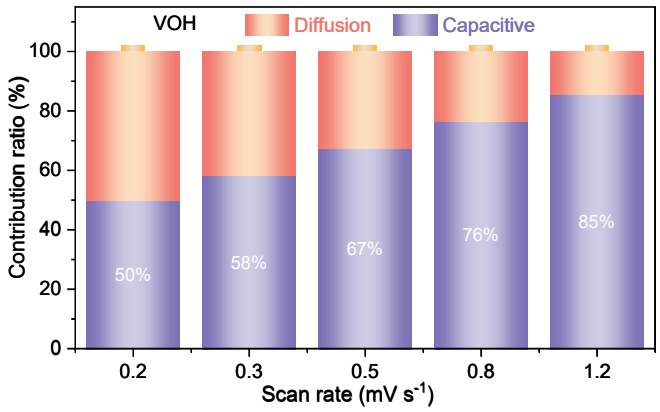

Fig. S17 Capacitive contribution of VOH at various scan rates.

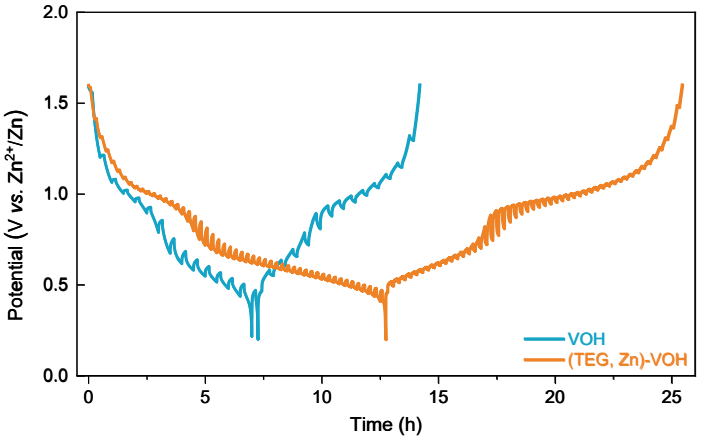

Fig. S18 GITT plots of VOH and (TEG, Zn)-VOH.

The relationship between Z' and $\omega^{-1/2}$ is $Z'=R_D+R_L+\sigma_\omega\omega^{-1/2}$.

The $D_{Zn^{2+}}$ can be calculated as following:

$$D_{Zn^{2+}}=\frac{R^2T^2}{2A^2n^4F^4C^2\sigma_\omega{}^2}$$

where R is the gas constant, T is the absolute temperature, A is the surface area, n is number of electrons transferred per molecule, F is the Faraday constant, C is ion concentration, D is the diffusion coefficient, and σ_ω is the Warburg coefficient.[9]

The $D_{Zn^{2+}}$ can be calculated from GITT:

$$D_{Zn^{2+}}=\frac{4}{\pi\tau}\left(\frac{m_BV_M}{M_BA}\right)^2\left(\frac{\Delta E_s}{\Delta E_\tau}\right)^2$$

where τ is the duration time, m_B is the mass of the active materials, V_M is the molar volume, M_B is the molecular weight, A is the contacting area, and ΔE_s and ΔE_τ are the change of steady-state voltage and overall cell voltage for the corresponding step, respectively.[10]

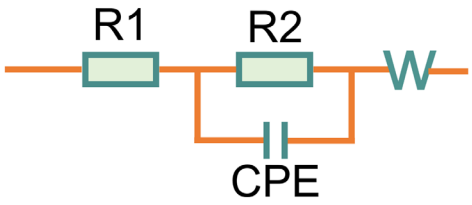

Fig. S19 The equivalent circuit.

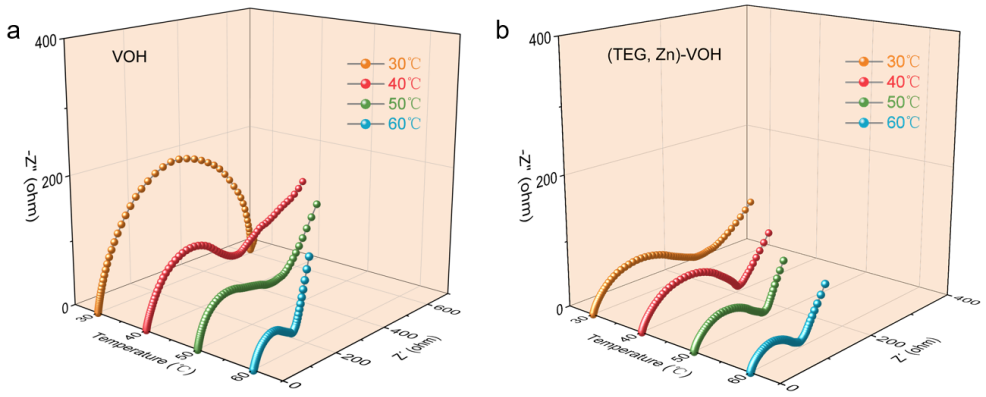

Fig. S20 EIS plots of a) VOH and b) (TEG, Zn)-VOH at different temperatures.

The activation energy (E_a) was determined according to the Arrhenius relationship:[11]

$$\frac{1}{R_{ct}} = A\exp\left(-\frac{Ea}{RT}\right)$$

Where R_{ct} is the charge-transfer resistance, A is the frequency factor, R is the gas constant, and T is the absolute temperature.

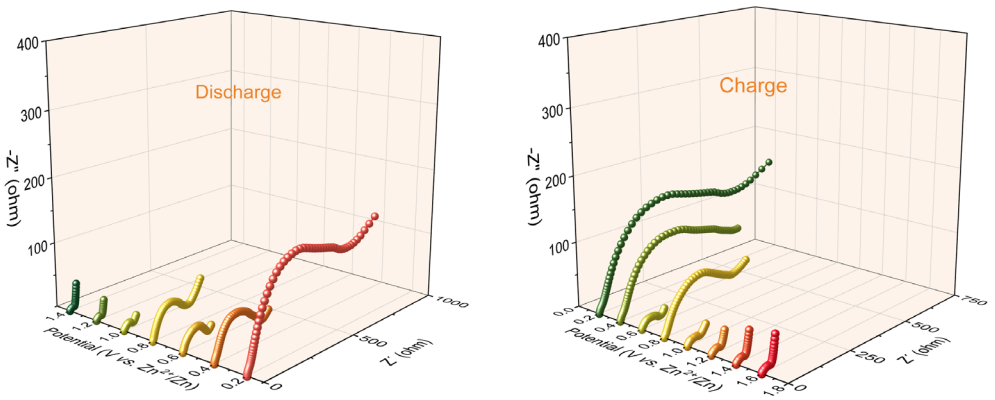

Fig. S21 In situ EIS plots of (TEG, Zn)-VOH.

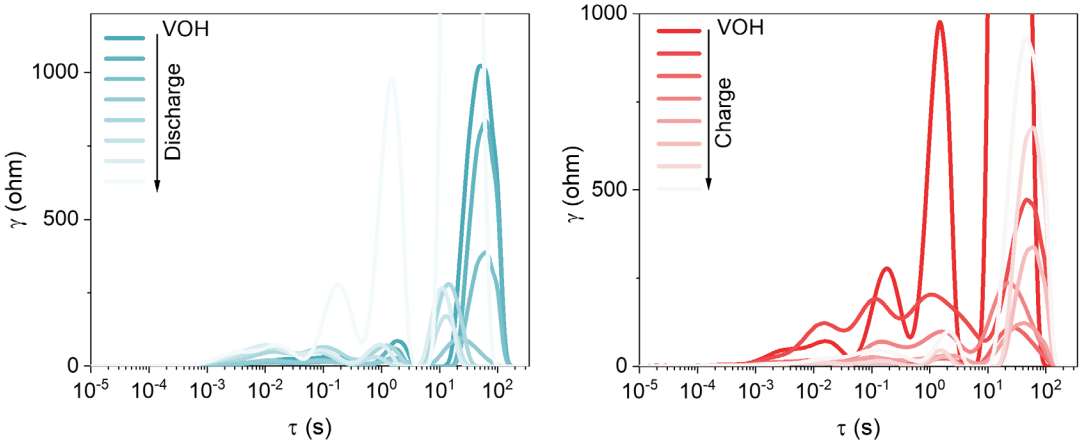

Fig. S22 In situ DRT of VOH.

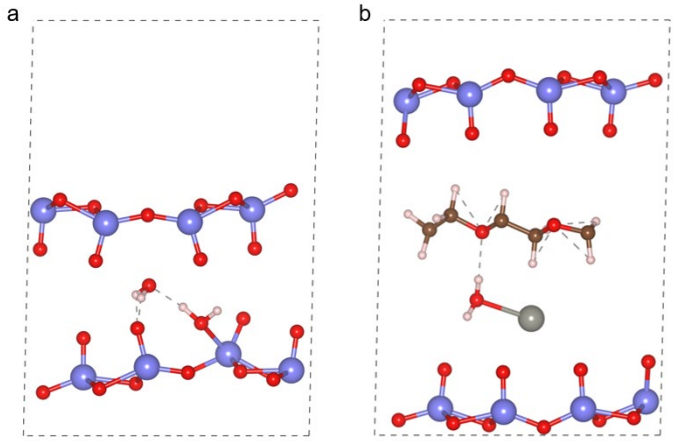

Fig. S23 Models for DFT.

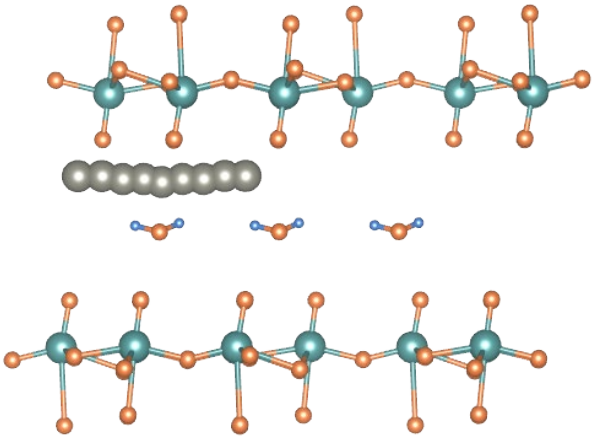

Fig. S24 Zn^{2+} pathway in VOH.

Table S1. ICP results of (TEG, Zn)-VOH.

Element	Cx (mg/kg)	W (%)
V	368034.0460	36.8034%
Zn	49825.0673	4.9825%

Table S2. Comparison of the electrochemical properties of (TEG, Zn)-VOH with those of the recently reported vanadium-based cathodes in aqueous ZIBs.

Materials	Capacity ($mAh\ g^{-1}$, $A\ g^{-1}$)	Rate capability ($mAh\ g^{-1}$, $A\ g^{-1}$)	Cycling performance	Ref.
(TEG, Zn)-VOH	460@0.1	301@5	106%, 10000 cycles, 10 $A\ g^{-1}$	This work
HAVO-DA	231.2@0.3	85.3@3	96.4%, 2500 cycles, 3 $A\ g^{-1}$	[12]
Sn-$V_3O_7{\cdot}H_2O$	408@0.1	187@5	89.3%, 6000 cycles, 5 $A\ g^{-1}$	[13]
NVO-Rb	463@0.1	152@5	87.6%, 10000 cycles, 10 $A\ g^{-1}$	[14]
MZVO	411@0.5	310@5	94%, 1000 cycles, 10 $A\ g^{-1}$	[15]
NVO/PoPDA@GO	433@0.5	224@5	74.9%, 1000 cycles, 5 $A\ g^{-1}$	[16]
PEO-LVO	438.1@0.1	230.1@5	89.8%, 3000 cycles, 10 $A\ g^{-1}$	[7]
HNVO-Glu	401@0.2	294@5	87.6%, 12000 cycles, 10 $A\ g^{-1}$	[17]
RuVO	405.8@0.2	289@5	98.2%, 5000 cycles, 10 $A\ g^{-1}$	[18]
CVO@PA/PPy	326.1@0.1	223.7@2.5	80.2%, 1000 cycles, 5 $A\ g^{-1}$	[19]
NiVO-BTA	464.2@0.2	272.5@5	88.8%, 1600 cycles, 5 $A\ g^{-1}$	[20]

References

[1] G. Kresse, J. Hafner, *Phys. Rev. B* **1993**, 47, 558.

[2] G. Kresse, J. Hafner, *Phys. Rev. B* **1994**, 49, 14251.

[3] J. P. Perdew, K. Burke, M. Ernzerhof, *Phys. Rev. Lett.* **1996**, 77, 3865.

[4] G. Kresse, D. Joubert, *Phys. Rev. B* **1999**, 59, 1758.

[5] P. E. Blöchl, *Phys. Rev. B* **1994**, 50, 17953.

[6] S. Grimme, J. Antony, S. Ehrlich, H. Krieg, *J. Chem. Phys.* **2010**, 132, 154104.

[7] M. Wu, C. Shi, J. Yang, Y. Zong, Y. Chen, Z. Ren, Y. Zhao, Z. Li, W. Zhang, L. Wang, X. Huang, W. Wen, X. Li, X. Ning, X. Ren, D. Zhu, *Adv. Mater.* **2024**, 36, 2310434.

[8] Q. Li, M. Xu, S. Wei, A. Kumar, K. K. Abdalla, Y. Wang, L. Yu, M. Liu, X. Jin, J. Li, L. Song, Y. Zhao, X. Sun, *Energy Environ. Sci.* **2025**, 18, 7939-7949.

[9] F. Wan, Z. Hao, S. Wang, Y. Ni, J. Zhu, Z. Tie, S. Bi, Z. Niu, J. Chen, *Adv. Mater.* **2021**, 33, 2102701.

[10] P. Hu, T. Zhu, X. Wang, X. Wei, M. Yan, J. Li, W. Luo, W. Yang, W. Zhang, L. Zhou, Z. Zhou, L. Mai, *Nano Lett.* **2018**, 18, 1758-1763.

[11] X. Lu, L. Chen, W. Li, X. Zhang, W. Chi, M. Peng, C. Wang, Y. Liu, X. Zhang, *Adv. Funct. Mater.* **2025**, e13457.

[12] Y. Zhang, S. Gao, Q. Li, Y. Sun, L. Jiang, Y. Su, S. Cao, H. Yue, H. Pang, *Adv. Funct. Mater.* **2025**, e22432.

[13] D. Zhang, J. Cao, C. Yang, K. Lolupiman, W. Limphirat, X. Wu, X. Zhang, J. Qin, Y. Huang, *Adv. Energy Mater.* **2024**, 15, 2404026.

[14] K. Wang, S. Li, X. Chen, J. Shen, H. Zhao, Y. Bai, *ACS Nano* **2024**, 18, 7311-7323.

[15] D. Dai, Y. Chen, B. Li, Z. Zhang, J. Wang, L. Wang, Y. Huang, B. Wang, D. H. Liu, *Small* **2024**, 21, 2408596.

[16] M. Li, M. Liu, Y. Lu, G. Zhang, Y. Zhang, Z. Li, Q. Xu, H. Liu, Y. Wang, *Adv. Funct. Mater.* **2024**, 34, 2312789.

[17] P. Zhang, Y. Gong, S. Fan, Z. Luo, J. Hu, C. Peng, Q. Zhang, Y. Li, X. Ren, *Adv. Energy Mater.* **2024**, 14, 2401493.

[18] Z. Chen, H. Liu, S. Fan, Q. Zhang, C. Yuan, W. Peng, Y. Li, X. Fan, *Adv. Energy Mater.* **2024**, 14, 2400977.

[19] H. Huang, X. Xia, J. Yun, C. Huang, D. Li, B. Chen, Z. Yang, W. Zhang, *Energy Storage Mater.* **2022**, 52, 473-484.

[20] J. Guo, J. Liu, W. Ma, Z. Sang, L. Yin, X. Zhang, H. Chen, J. Liang, D. Yang, *Adv. Funct. Mater.* **2023**, 33, 2302659.